VALIDATION OF A CAA FORMULATION BASED ON LIGHTHILL'S ANALOGY FOR A COOLING FAN AND MOWER BLADE NOISE

Robert SANDBOGE[1], Karl WASHBURN[2] and Chris PEAK[3]

[1] *Pioneer Solutions Inc., 143 Cadycentre #351, Northville, MI, 48167, USA*

[2] *John Deere Moline Technology Innovation Center, One John Deere Place, Moline, IL, 61265, USA*

[3] *John Deere SouthEast Engineering Center, 14401 Carowinds Blvd., Charlotte, NC, 28273, USA*

SUMMARY

A new implementation of a Computational Aeroacoustics formulation, based on Lighthill's Analogy, has been validated on two physical tests. The implementation involves sequential solutions, first of a static CFD, followed by a transient CFD, followed by the acoustical propagation. All of the solutions are performed using finite element methods, and the acoustic sources are integrated directly onto the acoustic mesh from within the CFD, not interpolated afterwards. The process is validated on both an engine cooling fan installed in a mock hood and cooling package, and on a single-blade, self-propelled, walk-behind lawn mower.

INTRODUCTION

A computational aero-acoustics (CAA) approach based on a variational formulation of Lighthill's analogy is validated for an axial fan application and a mower application. The CAA methodology is designed to be used on real world industrial applications where efficient evaluation of design proposals is critical. The control volumes used in the simulations are directly derived from the CAD models used in the product development process. A transient computational fluid dynamics (CFD) simulation with moving geometry is performed to compute acoustic noise sources. The noise sources are used in an acoustic wave propagation simulation to compute the acoustic field, which predicts the sound pressure level in the near field and the far field.

FIELD OF APPLICATION

Industrial off-road and commercial turf-care equipment tend to have significant aeroacoustic sources that strongly contribute to overall radiated sound power. In construction, forestry, and agricultural applications, engine cooling fans deliver sound powers that often dominate the total machine. In turf-care equipment, the mowing blades dominate the sound power. The engineering objective is to ensure that the noise levels in these systems are sufficiently low to allow the machines to pass international noise regulations. To date, there has been no simulation that can

reliably predict the sound power generated by such sources in situ. The purpose of this work is to evaluate a method in which a combined computational fluid dynamics (CFD) and computational aeroacoustics (CAA) technique is used to predict the noise level from an industrial engine cooling fan in an idealized engine compartment, and on the cutting blade of a single-deck, walk-behind lawnmower.

METHODOLOGY

The CAA technique uses an extended version of the variational formulation of Lighthill's analogy. This formulation is ideally suited to the finite element method (FEM). It accounts for aerodynamic sources through two source terms. The first term accounts for volume sources; the second term accounts for sources defined on control surfaces where the normal flow velocity does not vanish. We will present the multi-step FEM-based CFD process, which progresses from an initial static solution to a highly detailed time-domain solution including moving meshes around the blade circles. Care must be taken to ensure that aerodynamic sources are well accounted in the CAA simulation. Therefore, an important contribution of the present work is an innovative approach for transferring information from the CFD mesh to the co-resident FEM-based CAA mesh, which is typically of different extent and resolution. In this new approach, the CFD code directly computes the nodal quantities appearing in the variational formulation of Lighthill's analogy.

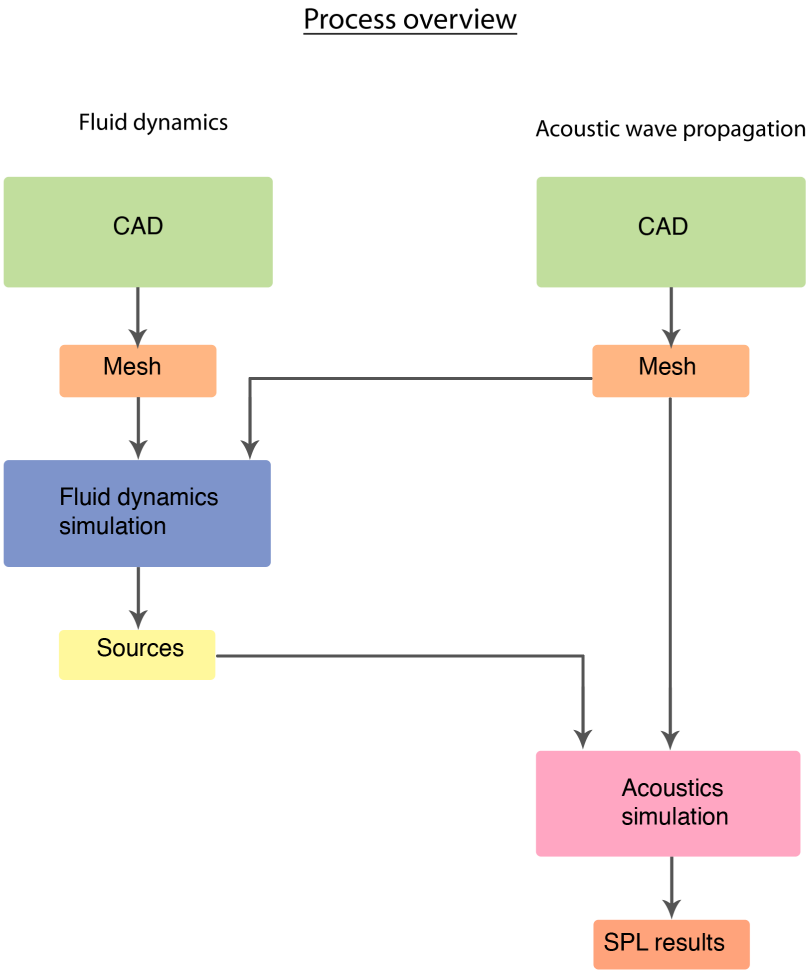

Figure 1. Schematic of the computation aeroacoustics implementation applied for this work. The simulation model is defined by the CAD models with its associated physical attributes and boundary conditions. The computed sound pressure level (SPL) is used in the validation.

The simulation process has two branches, one branch to compute the transient flow solution, and one branch to compute the acoustic response in and around the source region. An outline of the process is illustrated in Figure 1. Note that the CFD branch uses the mesh developed for the acoustic propagation in addition to the CFD mesh. The acoustic source terms computed in the CFD simulation are integrated on the acoustic mesh; this approach minimizes the numerical error associated with developing the acoustic sources from the flow computation.

The CAA methodology was developed in conjunction with Acusim Software, Inc. (AcuSolve FEM CFD solver), Free-Field Technologies, Inc. (Actran/LA FEM acoustics propagation solver) and Pioneer Solutions, Inc. (FluidConnection CAD integration and meshing software). John Deere supported the project with physical models and testing during the development phase.

THE COMPUTATIONAL AERO-ACOUSTICS FORMULATION

The aeroacoustic approach to predicting the sound radiating from rotating machinery uses an extension of the variational formulation of Lighthill's analogy [Lighthill], initially proposed in [Oberai1] and [Oberai2]. The proposed approach is well suited to treat flow noise problems with volumetric sources only. The ability to treat problems with sources on control surfaces was added in [Caro]. This addition makes it possible to solve problems with moving geometry, such as a mower or fan rotor, where the control surfaces enclose the moving parts. The CAA formulation is given below, where the following nomenclature is used:

δ_{ij}	Kronecker delta	i	index
φ	test fuction	j	index
Γ	boundary of domain	$\mathbf{n}$	normal
λ	second viscosity coefficient	p	pressure
μ	first viscosity coefficient	t	time
Ω	domain	T_{ij}	Lighthill's stress tensor
ϱ	density	$\mathbf{u}$	velocity vector
ϱ_0	density for air at rest	u_i	velocity component
$\varrho_a \equiv \varrho - \varrho_0$	acoustic density	x_i	spatial coordinate
Σ_{ij}	Total stress tensor		
τ	viscous stress tensor		

As indicated above, the overall CAA problem is based on two models: the Navier-Stokes equations to model the fluid dynamics and a wave equation based on the Lighthill's analogy. The Navier-Stokes equation can be written:

$$\frac{\partial \varrho}{\partial t} + \frac{\partial}{\partial x_i}(\varrho u_i) = 0, \text{ in } \Omega$$

$$\frac{\partial}{\partial t}(\varrho u_i) + \frac{\partial}{\partial x_j}(\varrho u_i u_j) = -\frac{\partial p}{\partial x_i} + \frac{\partial \tau_{ij}}{\partial x_j} \text{ in } \Omega,$$

$$p(t=0) = p_0 \text{ in } \Omega,$$

$$\mathbf{u}(t=0) = \mathbf{u_0} \text{ in } \Omega,$$

$$\mathbf{u} = \mathbf{u}_{\text{inlet}} \text{ or } p = -\frac{1}{2}\varrho(\mathbf{u}\cdot\mathbf{n})^2 \text{ on } \Gamma_{\text{inlet}},$$

$$\tau \cdot \mathbf{n} = \mathbf{0} \text{ and } p = 0 \text{ on } \Gamma_{\text{outlet}},$$

$$\mathbf{u} = \mathbf{u}_{\text{wall}} \text{ on } \Gamma_{\text{wall}},$$

where $\Gamma = \partial\Omega$, $\tau_{ij} = \mu\left(\frac{\partial u_i}{\partial x_j} + \frac{\partial u_j}{\partial x_i}\right) + \delta_{ij}\lambda\nabla\cdot\mathbf{u}$, p_0 and $\mathbf{u_0}$ are initial conditions, and $\mathbf{f}$ is a body force. If $\Gamma_{\text{inlet}} = \Gamma_{\text{outlet}} = \emptyset$, the pressure p is set to zero in a node away from source regions.

The wave equation can be derived by first taking time and spatial derivatives of the continuity equation and momentum equation respectively, and adding the terms together to obtain:

$$\frac{\partial^2}{\partial t^2}\left(\varrho-\varrho_0\right)-a_0^2\frac{\partial^2}{\partial x_i x_i}\left(\varrho-\varrho_0\right)=\frac{\partial^2 T_{ij}}{\partial x_i \partial x_j}$$

The Lighthill's tensor present in the right hand side is defined by:

$$T_{ij}=\varrho u_i u_j+\left(\left(p-p_0\right)-a_0^2\left(\varrho-\varrho_0\right)\right)\delta_{ij}-\tau_{ij}$$

In the second step, the right hand side tensor is decoupled from the acoustic density wave fluctuations, which leads to a proper wave equation:

$$\frac{\partial^2 \varrho_a}{\partial t^2}-a_0^2\frac{\partial^2 \varrho_a}{\partial x_i x_i}=\frac{\partial^2 T_{ij}}{\partial x_i \partial x_j}$$

It is now clear that it is possible to solve the Navier-Stokes equations and use the solution in a source term for a linear wave equation computing the acoustic density, by making the assumption that the acoustic fluctuations do not perturb the fluid dynamics solution. This is a reasonable assumption for the field of application presented here. The consequences are important, because it is very difficult to numerically compute the acoustic response directly from the Navier-Stokes equations; the scale of the acoustic wave fluctuations is much smaller than the scale of the fluid dynamics.

The computational methods are constructed from certain variational formulations. The CFD model is based on a DES (Detached Eddy Simulation - a combination of Large Eddy Simulation (LES) and Spalart-Allmaras turbulence models) formulation of Navier-Stokes, and the computational method is a Galerkin least squares finite element method, which is standard practice today for many applications. The details can be found in several places, see e.g. [Caro] or [Sandboge] for more details and references therein. The computational method for solving the wave equation is also a finite element method, and more details can be found in the same references. However, it is useful to know that there are two types of source terms present in the finite element formulation. This can be seen from the derivation of the weak variational formulation, which has the following form:

$$\int_\Omega\left(\frac{\partial^2 \varrho_a}{\partial t^2}\varphi+a_0^2\frac{\partial \varrho_a}{\partial x_i}\frac{\partial \varphi}{\partial x_i}\right)d\Omega=-\int_\Omega\frac{\partial T_{ij}}{\partial x_j}\frac{\partial \varphi}{\partial x_i}d\Omega+\int_\Gamma\frac{\partial \Sigma_{ij}}{\partial x_j}n_i\varphi d\Gamma\quad\forall\varphi$$

The source terms are present on the right hand side. The first term is integrated over a volume and involves the Lighthill's stress tensor defined above. The second term is integrated over surfaces and involves the tensor:

$$\Sigma_{ij}=\varrho u_i u_j+(p-p_0)\delta_{ij}-\tau_{ij}$$

The surface source term is zero for stationary walls and walls vibrating in-plane, but non-zero for control surfaces associated with moving geometry or surfaces that vibrate normal to their planes. Note that a control surface does not need to be a physical wall: it can be for instance a non-physical surface enclosing a source region. In that case it defines a boundary condition that captures the generated sound inside that particular volume.

VALIDATION

We present two validations of the CAA methodology discussed above. Simulations are compared with acoustical measurements, within anechoic chambers, performed at the Acoustics Laboratory at Iowa State University for the axial fan and at the John Deere SouthEast Engineering Center for the mower. The acoustic spectra predicted by the CAA process match well those measured experimentally.

Axial fan

The axial fan model was that of a seven-blade engine cooling fan used on a loader-backhoe, including the hood and obstructions similar to those found in the actual machine. Simulations were compared with physical experiments where the virtual simulation model mimicked the test mockup as closely as possible. In the CAD representation of the mockup, the only significant departure from the real geometry was for the heat exchanger, which was modeled as a simple block. This block was treated as a porous medium in the simulations, where the resistance was computed from heat exchanger core test data. An illustration of the test chamber (CAD model) is shown in Figure 2.

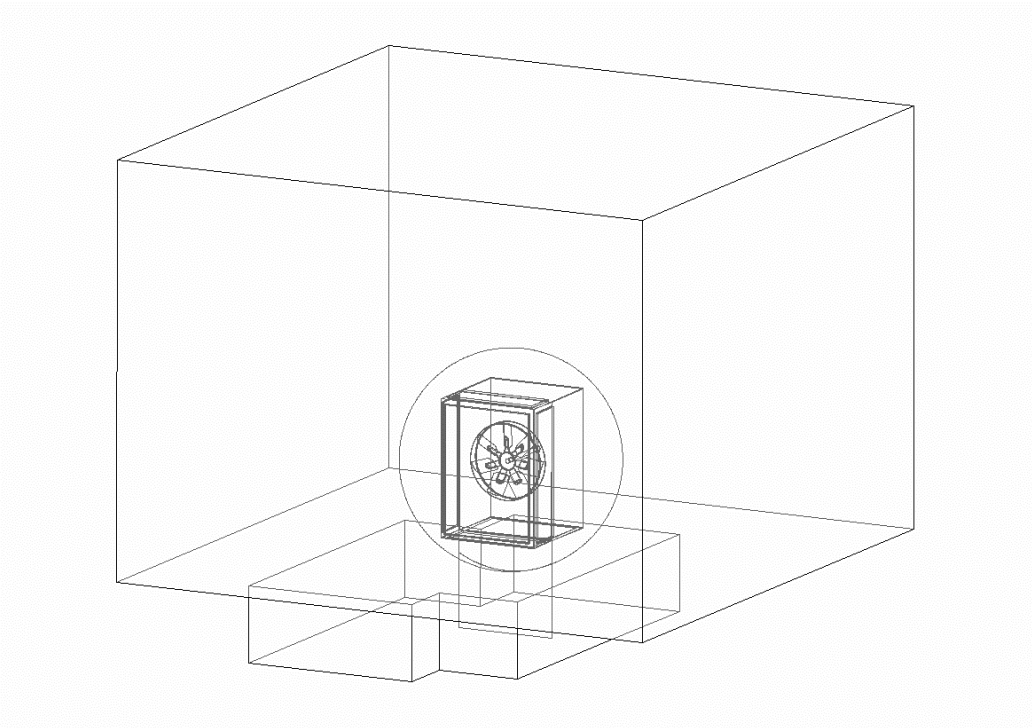

Figure 2. Line drawing of the anechoic test setup for the mock hood and cooling package housing the 7-blade axial flow engine cooling fan. The sphere at which the acoustic finite elements were mated to infinite elements is indicated by a circle.

The entire chamber volume is used for the FEM CFD simulations; a fine mesh is used close to the actual fan, and a coarse mesh is used further from the test rig. The fine mesh resolves large eddies using the LES turbulence model, while small eddies are modeled. To resolve the boundary layer close to walls, layers of flat elements are stacked using an advancing front meshing technique where the element size grows with the distance from the wall. By dynamically computing the frictional velocity at the walls in the simulations, a “wall function” is applied where and when needed to model a standard flat-plate velocity profile close to the walls. In all simulations, the wall spacing resolution was well within the requirements for the Spalart-Allmaras turbulence model, which was applied close to the walls in the simulations (LES was used away from the walls). The sphere outlined in the illustration shows the region where finite elements are used in the acoustic simulation, while the region outside the sphere is meshed with infinite elements. The use of infinite elements at a distance from the source regions works because the chamber walls do not reflect acoustic waves. The floor in a hemi-anechoic chamber is taken into account by adding the (complex) acoustic pressure at a particular point with the acoustic pressure at its mirrored point, where the floor acts as a mirror plane.

Initially, a steady state solution is computed using a basic turbulence model. The output provides initial conditions for the transient simulation. The system is solved for several thousand time steps

with a time step of $5 \cdot 10^{-5}$s to reach a pseudo-steady flow condition, and thereafter the acoustic sources are sampled for ten thousand or more time steps. Two simulations were performed on the axial fan, one at 1000 rpm and one at 2000 rpm. A snapshot of the velocity magnitude for the 2000 rpm case is shown in Figure 3, and static pressure for the same case is shown in Figure 4.

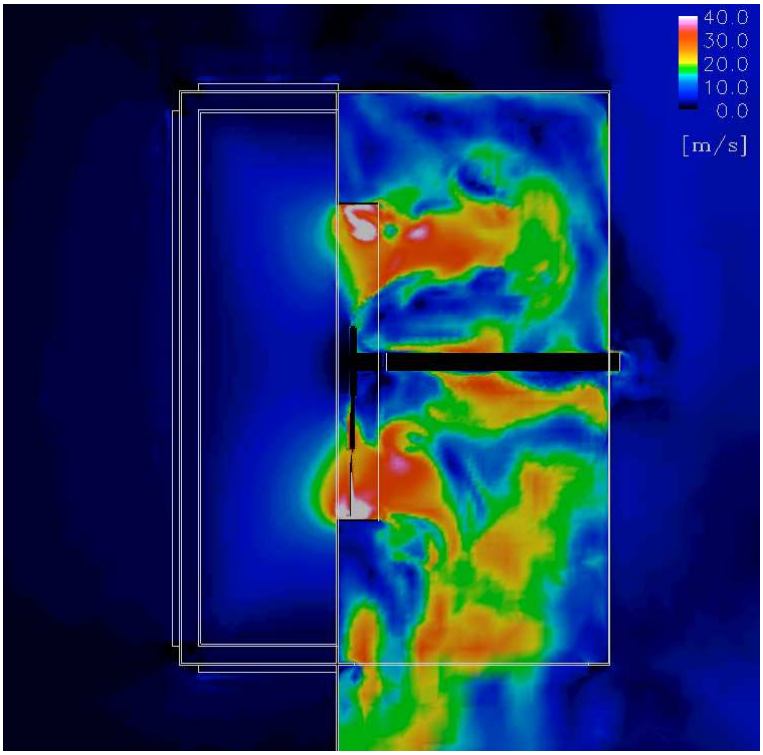

Figure 3. Velocity magnitude on a vertical plane intersecting the center of the fan axis, showing fully developed flow at a fan speed of 2000 RPM.

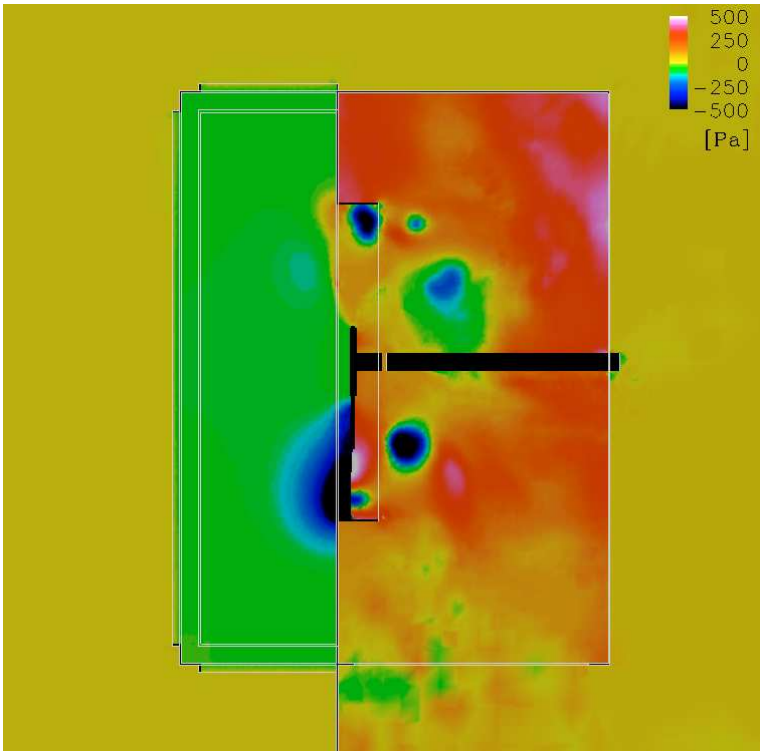

Figure 4. Static pressure on a vertical plane intersecting the center of the fan axis, showing fully developed flow at a fan speed of 2000 RPM.

Based on the source terms computed in the CFD simulation, the acoustic simulation propagates the response in the frequency domain. The sound pressure levels for the finite element solution at 200 Hz are shown in Figure 5 and at 600 Hz in Figure 6.

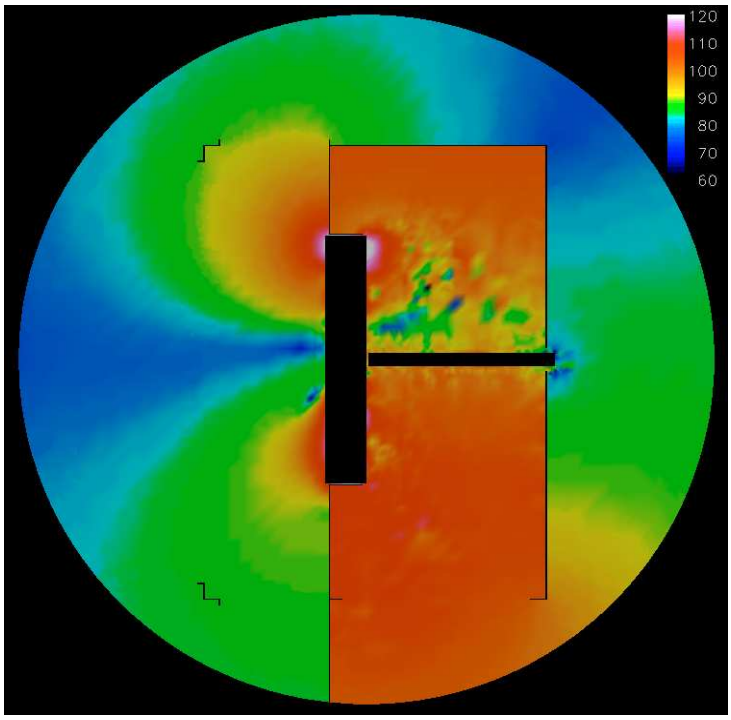

Figure 5. Sound Pressure Levels in decibels at 200 Hz on a vertical plane intersecting the center of the fan axis, at a fan speed of 2000 RPM.

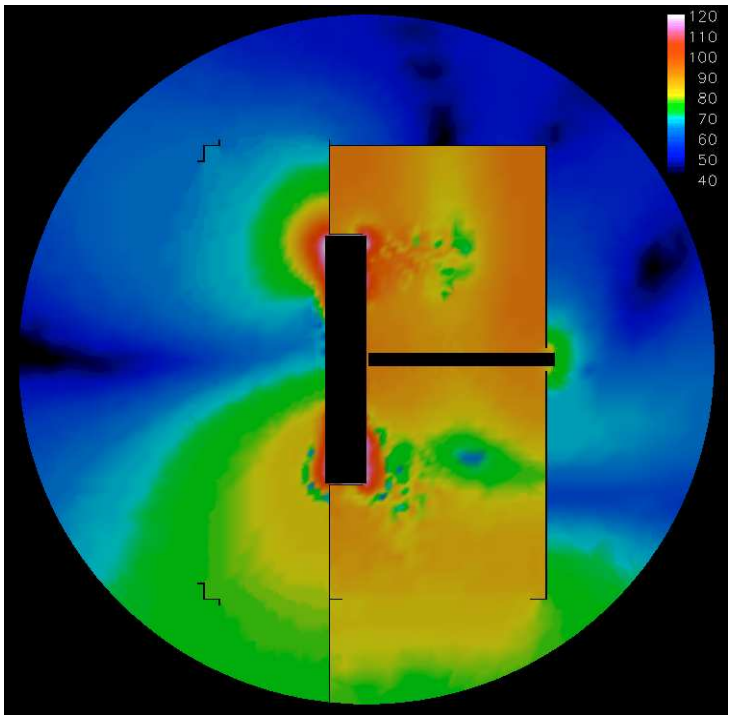

Figure 6 Sound Pressure Levels in decibels at 600 Hz on a vertical plane intersecting the center of the fan axis, at a fan speed of 2000 RPM.

The physical experiment measured the acoustic pressure at eight microphones, each at a distance of 1.5 meters from the fan. The same locations were used for the virtual microphones in the simulation. Similar sampling time was used in the physical experiments and the simulations to make comparisons easier. A comparison of the average response for the eight locations is shown in Figure 7 for a fan speed of 1000 RPM and in Figure 8 for a fan speed of 2000 RPM.

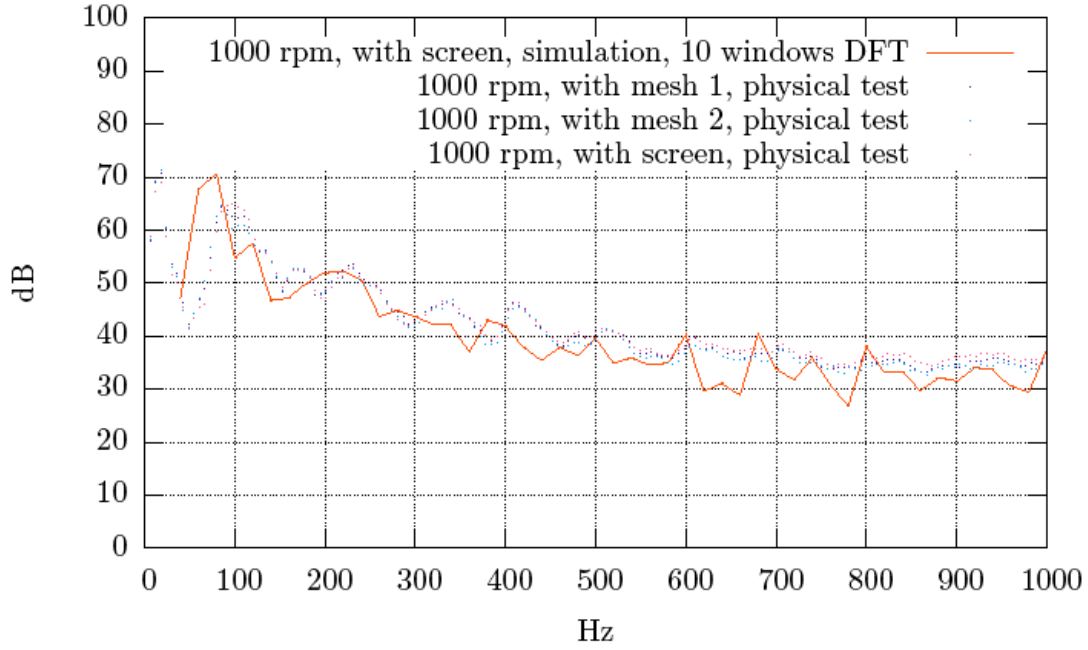

Figure 7 A comparison of the sound levels averaged over eight microphone locations surrounding the model at 1000 RPM fan speed. The solid curve is the CAA simulation; the dotted curves are multiple measurements in the anechoic chamber.

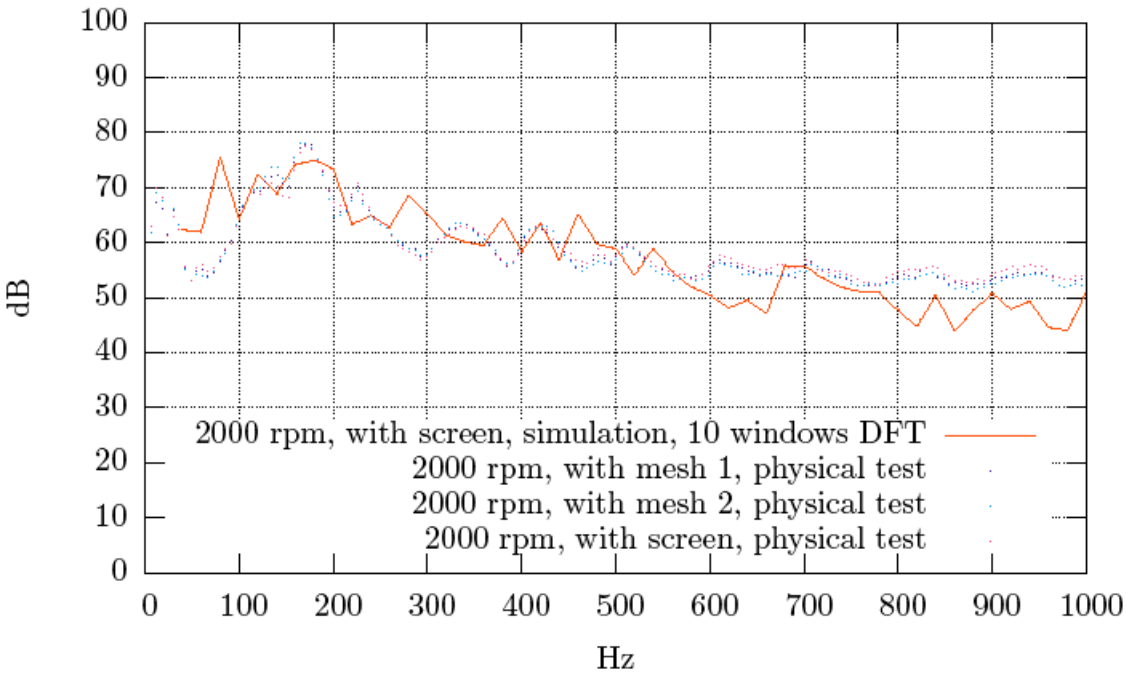

Figure 8. A comparison of the sound levels averaged over eight microphone locations surrounding the model at 2000 RPM fan speed. The solid curve is the CAA simulation; the dotted curves are multiple measurements in the anechoic chamber.

Mower

The procedure for the mower experiments and simulations was similar to the fan tests. The impeller was driven by an electrical motor which produced minimal noise levels. The test was performed in a hemi-anechoic chamber with a hard floor. The floor was assumed to reflect all acoustic waves without loss in the simulations.

A snapshot of isosurfaces of the divergence of the Lighthill's tensor is shown in Figure 9, indicating that noise is generated around and behind the blades.

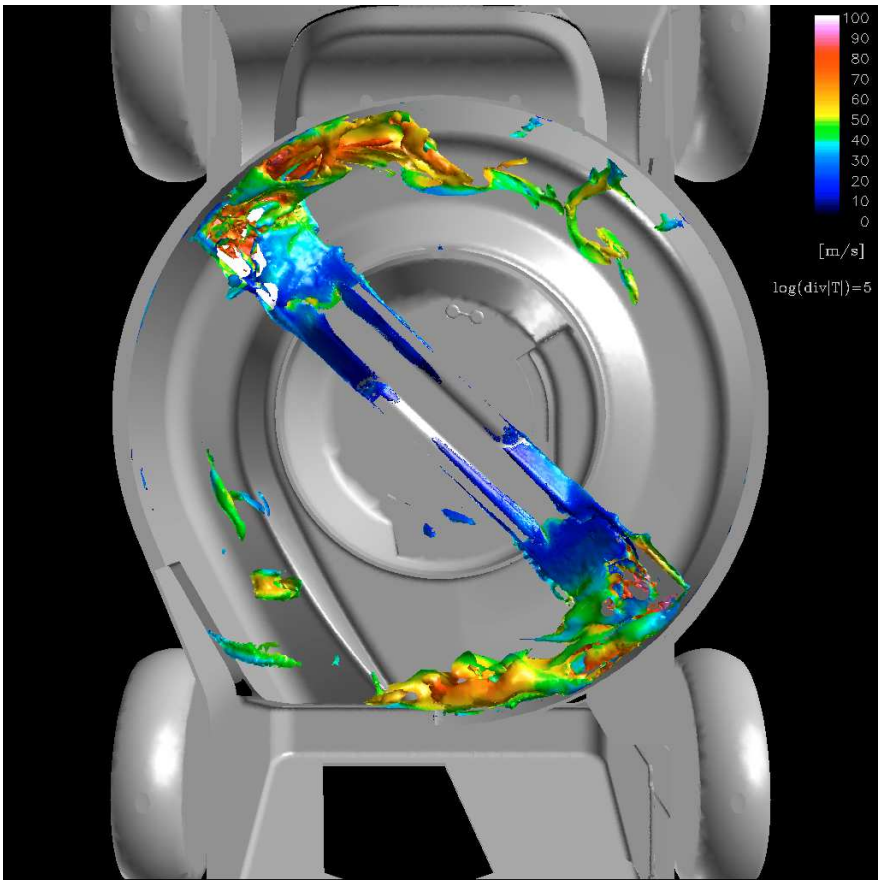

Figure 9. Isosurfaces of constant divergence of Lighthill's tensor (proportional to acoustic source strength), false-colored in velocity magnitude, for the blade underneath the mower deck. The blade is rotating counter clock-wise at 3000 RPM.

The sound pressure level for the acoustic field around the mower at 100 Hz is shown in Figure 10, and at 1000 Hz in Figure 11.

Two different meshes were used for the CFD simulations, a coarse mesh with 8 million tetrahedra and a fine mesh with twice as many elements. The meshing strategy is the same as for the fan model above and follows the principles suitable for the DES turbulence model. The mesh was finer around the rotor in both cases, and a very coarse mesh was used away from the source region. The time step was $5 \cdot 10^{-5}$s for both meshes. The results, in Figures 12 and 13, were averaged from 12 microphone locations, all at a distance 1.5 m from the center of the rotor evenly distributed around the mower, and similar sampling time was used for all cases.

Note that the narrowband Blade Passage Frequency (BPF) tone (100 Hz) and three of its prominent harmonics are accurately captured by the simulation. This was a key goal of the new CAA methodology. Likewise, the turbulent spectrum is modeled well from about 50 Hz to about 1400 Hz. This band represents about 95% of the overall sound power generated by the mower blade.

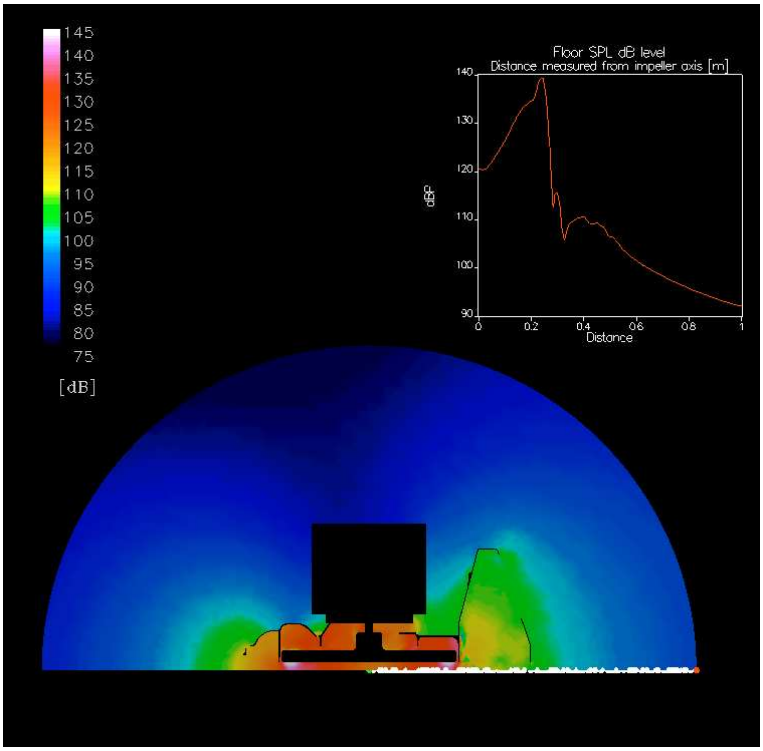

Figure 10. Radiated sound pressure level in dB under and outside of the mower deck at 100 Hz, shown on a vertical plane through the center of the mower.

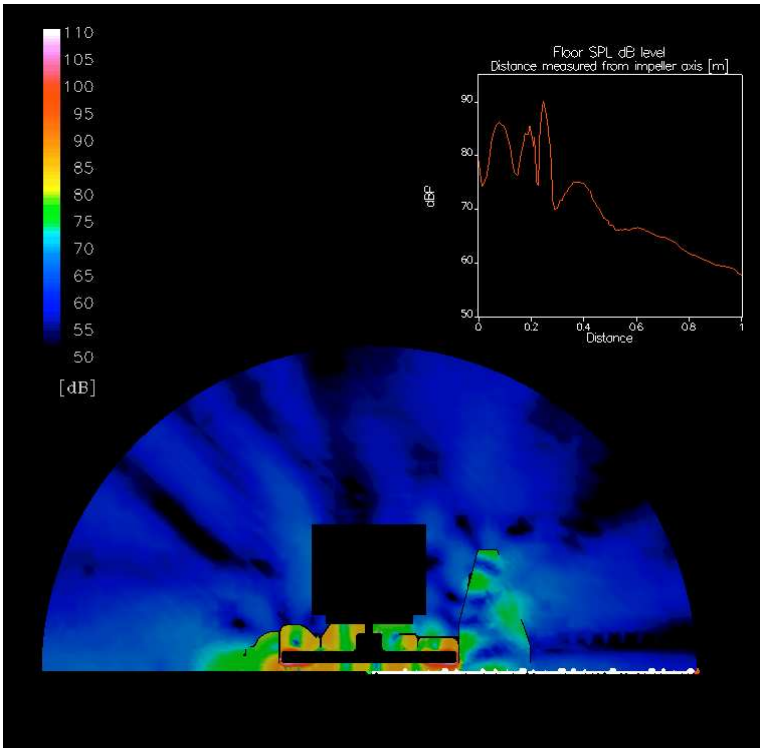

Figure 11. Radiated sound pressure level in dB under and outside of the mower deck at 1000 Hz, shown on a vertical plane through the center of the mower.

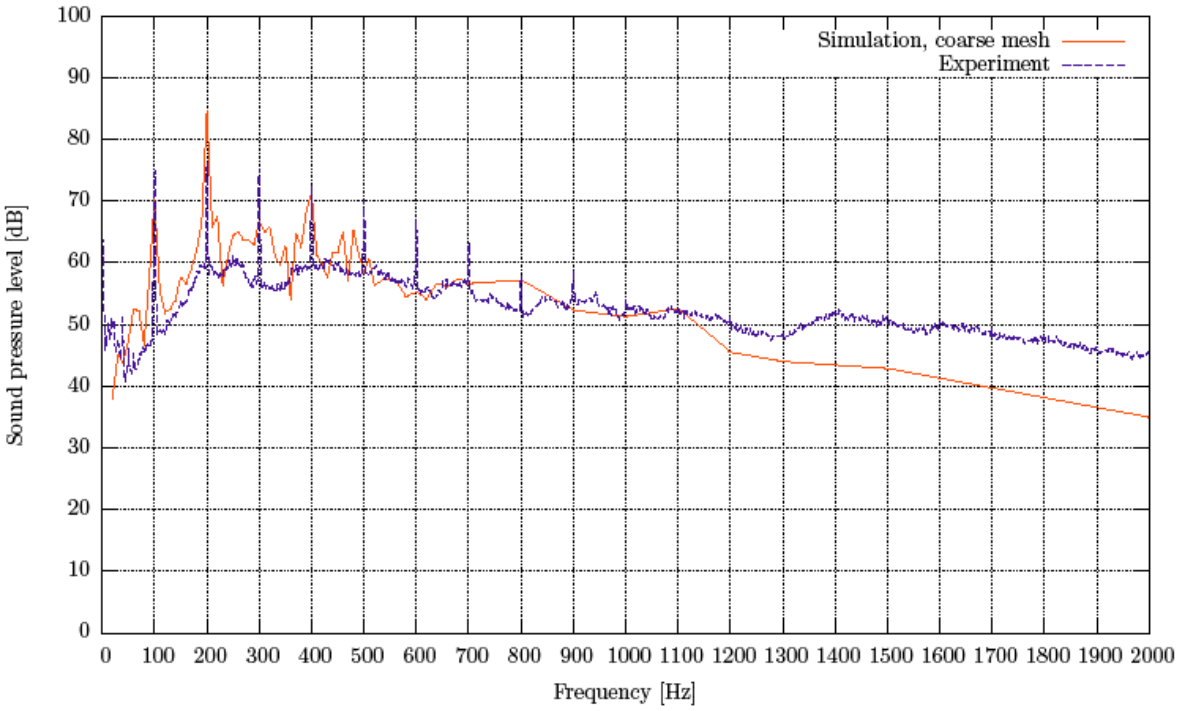

Figure 12. A comparison of the sound levels averaged over eight microphone locations surrounding the model. The red curve is the CAA simulation; the blue curve is the measurement in the anechoic chamber. The CFD mesh consisted of 8 million tetrahedra.
The results begin to deviate at about 1100 Hz.

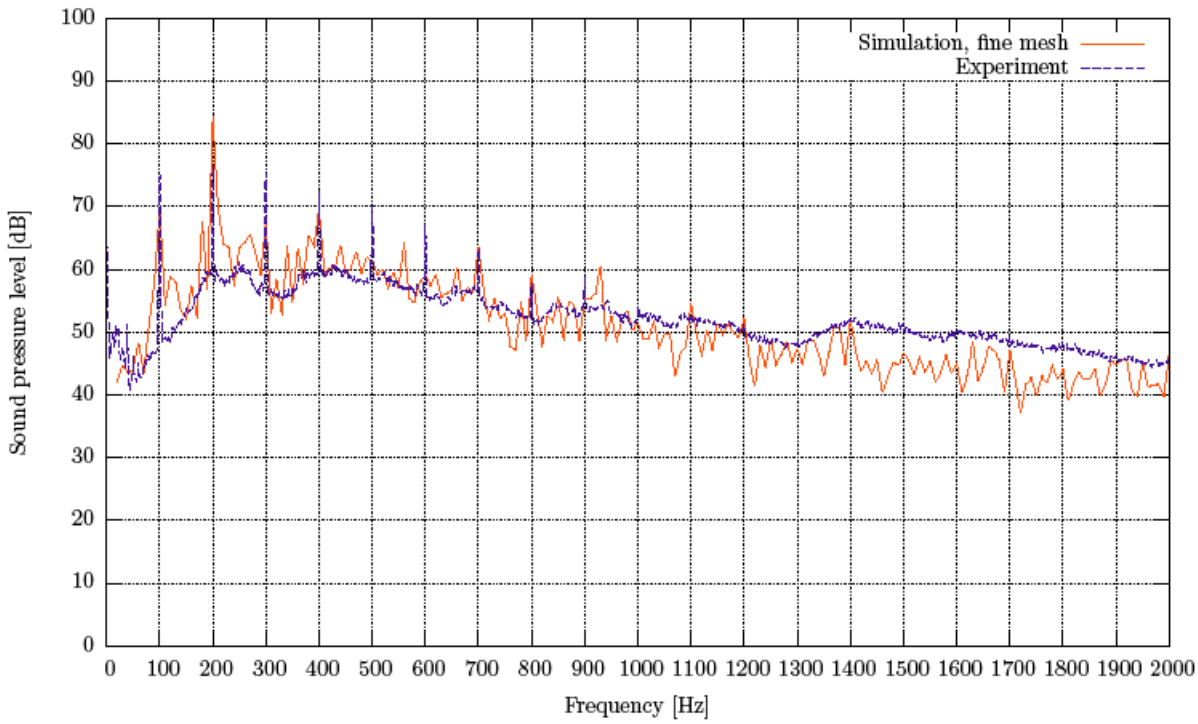

Figure 13. A comparison of the sound levels averaged over eight microphone locations surrounding the model. The red curve is the CAA simulation; the blue curve is the measurement in the anechoic chamber. The CFD mesh consisted of 16 million tetrahedra and
the results agree better out to about 1400 Hz.

CONCLUSION

The comparison of the presented CAA simulation methodology with physical experiments shows excellent agreement for frequencies up to roughly 1400 Hz (using 16 million tetrahedra), which is the most important range for these applications. It is possible to move to higher frequencies as well using this approach; this requires the use of finer meshes to resolve frequencies higher than those demonstrated in this work. The model also correctly captured the Blade Passage Frequency tone and most of its important harmonics. The simulations predict actual sound levels for rotating aeroacoustic sources, as well as provide valuable nearfield information that can be easily visualized. The field plots show that source strength is large close to the tip of the rotor blades and contribute to noise at blade passing frequencies and higher frequencies. Dynamic animations show in detail flow mechanisms responsible for noise creation. E.g., the mower blade tip creates vortices as it passes the clipping exhaust, leading to high Lighthill's tensor amplitudes and noise source creation.

ACKNOWLEDGEMENTS

The analyses were carried out using Pro/Engineer CAD [PTC], FluidConnection [Pioneer], AcuSolve [Acusim], Actran/LA [FFT], Fieldview [Ilight] and gnuplot [GNU].

REFERENCES

[Acusim] *AcuSolve™ CFD solver*, Acusim Software, Inc., 2685 Marine Way, Suite 1215, Mountain View, CA 94043, USA, www.acusim.com.

[Caro] Caro S., Ploumhans P., Gallez X., Sandboge R., Shakib F., and Matthes M. – *A New Formulation based on Lighthill's Analogy applied to an Idealized Automotive HVAC Blower using AcuSolve and Actran/LA*, AIAA/CEAS 11th Aeroacoustic Conference, 23-25 May 2005, Monterey, California, USA, AIAA Paper 2005-3015 (**2005**).

[FFT] *Actran 2004 Aeroacoustic Solutions: Actran/TM and Actran/LA - User's Manual*, Free-Field-Technologies-S.A., 16, place de l'Universite', 1348 Louvain-la-Neuve, Belgium, (**2004**).

[GNU] *Gnuplot plotting utility*, www.gnuplot.info.

[Ilight] *Fieldview visualizer*, Intelligent Light, 1290 Wall Street West, Lyndhurst, NJ 07071, USA, www.ilight.com.

[Lighthill] Lighthill M. – *On Sound Generated Aerodynamically*, Proc. Roy. Soc., London, Vol. A 211 (**1952**).

[Oberai1] Oberai A., Ronaldkin F., and Hughes T. – *Computational Procedures for Determining Structural-Acoustic Response due to Hydrodynamic Sources*, Comput. Methods Appl. Mech. Engrg., Vol. 190, pp. 345-361 (**2000**).

[Oberai2] Oberai A., Ronaldkin F., and Hughes T. – *Computation of Trailing-Edge Noise due to Turbulent Flow over an Airfoil*, AIAA Journal, Vol. 40, pp. 2206-2216 (**2002**).

[Pioneer] *FluidConnection 2.0 User Guide*, Pioneer Solutions Inc., 143 Cady Centre \#251, Northville, MI 48167, USA (**2007**).

[PTC] *Pro/E™*, Parametric Technologies Corp., 128 Technology Dr., Waltham, MA 02154, USA.

[Sandboge] Sandboge R., Caro S., Ploumhans P., Ambs R., Schillemeit B., Washburn K.B., Shakib F. – *Validation of a CAA Formulation Based on Lighthill's Analogy Using AcuSolve and Actran/LA on an Idealized Automotive HVAC Blower and on an Axial Fan*, AIAA/CEAS 12th Aeroacoustic Conference, 8-10 May 2006, Cambridge, Massachusetts, USA (**2006**).